J Mater Sci: Mater Med (2008) 19:2845–2850
DOI 10.1007/s10856-008-3411-8

Sonoelectrochemical deposition of calcium phosphate coatings on carbon materials—effect of electrolyte concentration

H. M. Han · G. J. Phillips · S. V. Mikhalovsky · S. FitzGerald · A. W. Lloyd

Received: 21 December 2007 / Accepted: 19 February 2008 / Published online: 14 March 2008

Abstract Calcium phosphate was deposited on carbon materials using a sonoelectrochemical method in an electrolyte containing calcium and phosphate ions. The effect of electrolyte concentration on sonoelectrochemically deposited calcium phosphate coatings was investigated and the underlying deposition mechanisms were discussed. The morphology, size and composition of the crystalline deposits changed with the electrolyte concentration. A mixture of plate, sphere and needle-like deposits was obtained at Ca^{2+} ion concentrations greater than 16 mM, however needle-like hydroxyapatite (HA) was obtained at lower Ca^{2+} concentrations. Analysis revealed that the sonoelectrochemical deposition of calcium phosphate consists of two processes—nucleation and crystal growth. The results suggest that the homogeneous nucleation of calcium phosphates in solution, followed by their absorption onto the carbon surface may account for the mechanism of coating observed at higher ionic concentrations. At lower concentrations, heterogeneous nucleation occurs on the surface of the carbon fibres, followed by the development of islands of crystal growth. The lower ionic concentration was shown to favour the generation of hydroxyapatite on carbon-based materials.

H. M. Han
Department of Chemistry and Chemical Engineering, ZhongKai University of Agriculture and Technology, Guangzhou 510225, China

H. M. Han (✉) · G. J. Phillips · S. V. Mikhalovsky · A. W. Lloyd
Biomedical Materials Research Group, School of Pharmacy and Biomolecular Sciences, University of Brighton, Brighton BN2 4GJ, UK
e-mail: xyzhhm@sina.com; h.han@brighton.ac.uk

S. FitzGerald
HORIBA Jobin Yvon Ltd, Middlesex HA7 1BQ, UK

1 Introduction

Carbons have previously been considered as suitable materials for both hard and soft tissue implants due to their exceptional mechanical properties including flexural and fatigue strength and high strength-to-weight ratio. However, the low biological activity of carbon currently restricts its use in biomedical applications [1, 2]. Calcium phosphate (CaP) ceramics, especially hydroxyapatite (HA), have received much attention in the biomedical materials field and have been clinically applied as coatings in orthopaedics and dentistry as a consequence of their excellent cyto-compatibility, bioactivity and osteoconductivity [3]. Carbon fibre-reinforced HA composites, in which the highly cyto-compatible but mechanically weak ceramic matrix is reinforced with carbon fibres, may provide bioceramic materials which can be used in the re-construction of bone defects [4].

The techniques used to produce calcium phosphate on implant surfaces have attracted considerable attention in the past decade [3, 5]. The techniques including plasma spraying, magnetron sputtering, pulsed laser deposition (PLD), radio-frequency sputtering, and thermal spraying et al. involve high temperature processing. They can deliver CaP only to the outer pore surfaces of the substrates and they are not effective in coating the substrates' inner pore surfaces. Other techniques, such as biomimetic deposition and electrodeposition, utilise lower temperatures and avoid the challenge associated with the structural instability of the products at elevated temperatures. Additionally, the calcium phosphates obtained at lower temperatures exhibit structures more similar to those of the natural bones. Compared with biomimetic deposition which requires only immersion of the surfaces to be coated in an aqueous solution of supersaturated calcium and

phosphate, the electrodeposition is aided by electrochemical reactions on the substrate surfaces in electrolytes containing calcium and phosphate ions, which is able to deposit a CaP layer on the inner pore surfaces at a higher speed [6–9]. Apparently, electrochemical deposition is especially useful for calcium phosphate coatings on substrates having a complicated shape such as dental implant and orthopaedic fixation devices. A recent and useful approach has been sonoelectrochemistry the combination of ultrasound with electrochemistry, which provides various benefits over conventional, (so-called silent) electrodeposition. Sonoelectrochemical deposition has previously been reported to increase the hardness and thickness of the ceramic coating, markedly improve deposition rates and efficiencies, and enhance adhesion of the coating to the substrate [10–14].

We have demonstrated that uniform, bioactive calcium phosphate coatings are produced on carbon fabric surfaces using a sonoelectrochemical method [15]. It is well known that the properties of electrochemical coatings are dependent on the electrolyte composition, including ionic concentration, initial pH, and reaction temperature [10, 11]. The application of ultrasound, combined with electrochemical deposition is a more complex process but it is still dependent on electrolyte related variables, in addition to those introduced by the application of sound. The aim of this study was to investigate the effect of altering the ion concentration of the electrolyte on the morphology and structure of the calcium phosphate coatings generated using sonoelectrochemical deposition on carbon cloths.

2 Materials and methods

An electrochemical cell, placed in a Fisher Brand 11002 ultrasonic bath, was configured to use carbon fabrics, standard product derived from C-Tex 13 (MAST Carbon Advanced Products Ltd., UK), as the working electrode and a platinum plate for the counter electrode. The electrolyte used for the fabrication of phosphate coatings was produced by dissolving reagent grade $Ca(NO_3)_2{\cdot}4H_2O$ and $NH_4H_2PO_4$ in deionized water, with the ion concentrations as listed in Table 1.

The pH of the electrolyte solution was adjusted to 5.5 using NH_4OH. The current density was maintained constant at 20 mA/cm^2 using a PGSTAT12 potentiostat during the process. Phosphate coatings were deposited on the cathode (carbon fabric sample) at 50°C for 45 min. The intensity and frequency of the ultrasound were set at 2.16 W/cm^2 and 40 KHz respectively.

Table 1 Ion concentrations of the electrolyte

Ca^{2+} (mM)	6	10	16	26	42
HPO_4^{2-} (mM)	3.6	5.9	9.6	15.5	25

Scanning electron microscopy (SEM), Raman and Fourier transform infra-red (FTIR) spectroscopy were applied as the main tools for the characterisation of precipitates on the carbon substrates. The phosphate morphology was examined under a JEOL JSM-6310 scanning electron microscope. Prior to analysis the samples were coated with palladium (Pd). The FTIR spectra were recorded in the 500–4,000 cm^{-1} range, with a resolution of 4 cm^{-1}, using an AVATAR 320 FTIR Nicolet Golden Gate ZnSe spectrometer. The Raman scattering measurements were performed using a HORIBA Jobin Yvon LabRAM HR dispersive Raman microscope. Excitation was provided by an integrated 633-nm helium–neon laser providing 10 mW at the sample. Spectra were collected through LabSpec software, using an air cooled CCD detector.

3 Results

Figure 1 shows SEM micrographs of the calcium phosphate deposits produced at the different ionic concentrations. It is clear that at Ca^{2+} ion concentrations greater than 16 mM the resulting coating consisted of a number of different forms, including plates, spheres and needles. As the Ca^{2+} concentration is reduced to 10 and 6 mM, the deposits exhibit completely different morphologies. The crystals are of smaller size, with a needle-like shape, resulting in a denser and more uniform coating. Moreover, large amounts of white precipitate were observed to form in the electrolyte when the Ca^{2+} ion concentration exceeded 16 mM, while the electrolyte remained clear at lower Ca^{2+} ion concentrations (10 and 6 mM).

The FTIR spectra are shown in Fig. 2. The bands around 1,400 cm^{-1} are assigned to carbonate (CO_3^{2-}), and the bands at 872 cm^{-1} can be attributed to HPO_4^{2-} or CO_3^{2-}. The bands at 1,024 cm^{-1} is associated with the v_3 vibration of PO_4^{3-} while those at 962 cm^{-1} represent the v_1 vibration of PO_4^{3-}, which is typical of hydroxyapatite (HA). The bands at 602 and 561 cm^{-1} are assigned to v_4 vibrations of the phosphate group (triply degenerated bending mode). The weak bands at 711 cm^{-1} are due to the existence of the CO_3^{2-} in $CaCO_3$ [16].

It is apparent from Fig. 3 that as the Ca^{2+} concentration of the electrolyte was reduced from 42 to 6 mM, the band intensities corresponding to the functional group CO_3^{2-} and HPO_4^{2-} decreased. The band intensities relating to PO_4^{3-} (1,024, 962, 602, 561 cm^{-1}), however, increased with a reduction in the calcium ion concentration, with the greatest peak intensity seen at 10 mM Ca^{2+}. Further

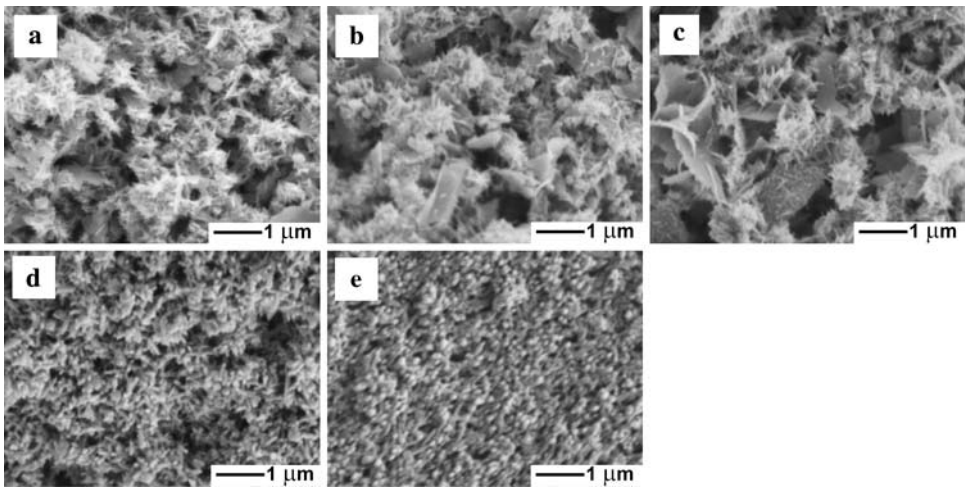

Fig. 1 SEM micrographs of the samples prepared by the sonoelectrodeposition with the different electrolyte concentrations: (**a**) 42 mM Ca^{2+}; (**b**) 26 mM Ca^{2+}; (**c**) 16 mM Ca^{2+}; (**d**) 10 mM Ca^{2+}; and (**e**) 6 mM Ca^{2+}

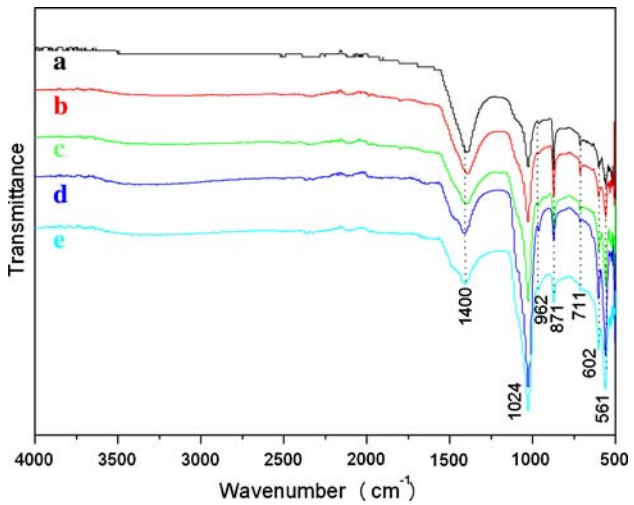

Fig. 2 FTIR spectra of the samples prepared by the sonoelectrodeposition with the different electrolyte concentrations: (**a**) 42 mM Ca^{2+}; (**b**) 26 mM Ca^{2+}; (**c**) 16 mM Ca^{2+}; (**d**) 10 mM Ca^{2+}; and (**e**) 6 mM Ca^{2+}

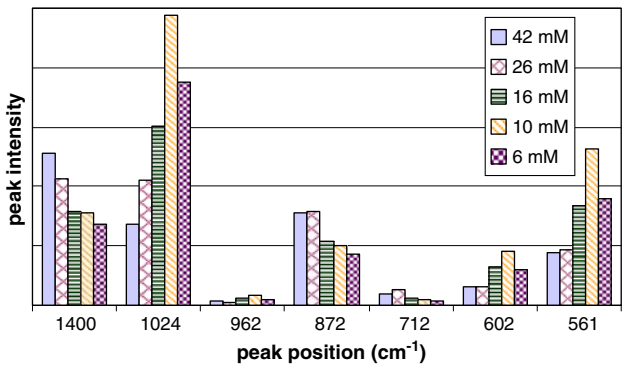

Fig. 3 Peak intensities at some particular wave numbers in FTIR spectra of the samples prepared by the sonoelectrodeposition with different electrolyte concentrations

reduction in the electrolyte concentration to 6 mM resulted in a decrease in the band intensity relating to PO_4^{3-}.

The Raman spectra, shown in Fig. 4, confirm that two main components were present in the coating. The peaks at 961 cm^{-1}, with other weak peaks at 431, 588, and 1,074 cm^{-1} correspond to a calcium phosphate species, possibly HA, as shown in Fig. 4a. The peaks present in Fig. 4b at 276, 712, and 1,084 cm^{-1}, are characteristic of calcium carbonate ($CaCO_3$). The double peaks at 1,315 and 1,600 cm^{-1} correspond to carbon substrates. With the change in Ca^{2+} ion concentration from 6 to 42 mM, the broadening of the 961 cm^{-1} band (Fig. 4c) indicates a change in phase/crystallinity of the coatings. Furthermore, the Raman chemical image of the three-dimensional representation of the deposit distribution (Fig. 4d) displays the 'islands' on the substrate, inferring the growth of nucleated crystals on the surface.

4 Discussion

The formation of crystals in liquid solutions begins with nucleation [17], which depends on the supersaturation of the system. It has previously been demonstrated that in electrochemical cells, the deposition of calcium phosphate on the cathode is induced by the super-saturation of calcium phosphate salts [11]. The ultrasound used in the present study, 40 kHz in frequency and 2.16 W/cm^2 in intensity, was assumed to induce identical effects considering that the samples and electric cell were located same as possibly during the processes [18, 19]. It can, therefore, be assumed that the mechanisms of sonoelectrodeposition of calcium phosphate coatings should be similar to those seen in traditional electrodeposition (without sonication), i.e. comprising of two processes: nucleation and crystal growth [11, 20].

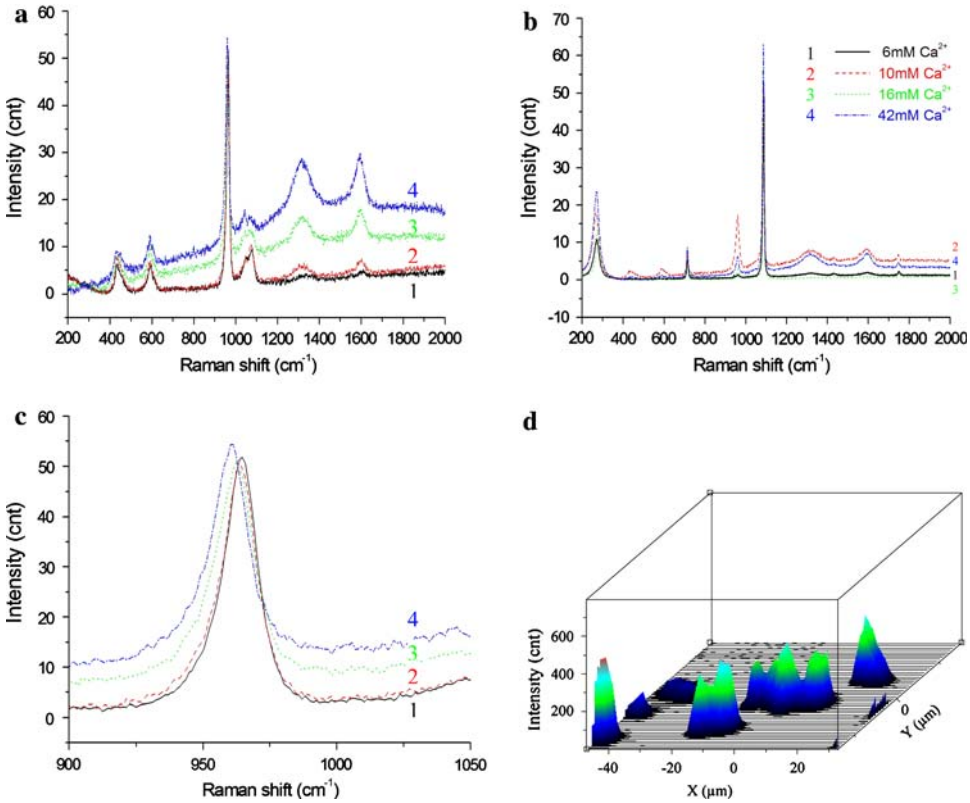

Fig. 4 Raman spectra and chemical image showing (**a**) the spectra bands at the 961 cm^{-1}; (**b**) the spectra bands at 1,084 cm^{-1}; (**c**) the enlarge view of the bands at 961 cm^{-1}; and (**d**) 3D representation of the deposition distribution

The first step of the CaP sonoelectrodeposition begins with nucleation. According to classical thermodynamic nucleation theory, the driving forces for nucleation can be calculated by the free energy change in supersaturated solutions:

$$\Delta G = -\frac{RT}{n}\ln S \tag{1}$$

$$S = c/c^* \tag{2}$$

where ΔG is the Gibbs free energy per mole of ionic units that compose Ca-P in solution, R is the universal gas constant, T is the absolute temperature, n is the number of ion units in a-Ca-P molecule and S is the supersaturation that can be defined by the ratio of the actual solution concentration (c) to the equilibrium saturation concentration at the same temperature (c*) when the solution is diluted enough [17].

On the other hand, from the kinetics viewpoint, the nucleation rate in aqueous solution, J, may be expressed as

$$J = A\exp\left[-K(\log S)^{-2}\right] \tag{3}$$

in which A and K are two constants depending on the physical properties and hydrodynamics of the system [17]. It can be deduced from the equations above that the nucleation strongly depends on the supersaturation of the solution if other parameters are assumed to be unchanged.

In this study, the only variable experimental parameter is ion concentration. As the concentration increases, according to the function (2), the supersaturation degree of solution goes up, and the change in supersaturation therefore affects Gibbs free energy ΔG and nucleation rate J of CaP formation, specifically a reduced free energy and a faster formation of CaP nuclei.

Kashchiev and colleagues have previously demonstrated that while heterogeneous nucleation (HEN) is prevalent at lower supersaturations, at higher supersaturations homogeneous nucleation (HON) is the dominant process, despite the presence of impurities in the solution [17]. In addition, it is reported that CaP precipitates form in acidic solutions when the ion concentration of calcium exceeds 12 mM [21]. Therefore it is reasonable to conclude that, in our experimental conditions, the rapid formation of CaP precipitate in the electrolyte at higher concentrations (>16 mM; pH 5.5), is attributed to the HON resulting from the higher supersaturation. In the samples run at lower concentration, the formation of the CaP deposits may be attributed to the heterogeneous nucleation (HEN) model. The formation of the CaP is schematically shown in Fig. 5.

Once formed the nuclei will coalesce and grow. Small islands are formed on the substrate surface (Fig. 4d) under the HEN condition. Following the increase in island density and size, the substrate materials are covered by a CaP layer [22]. On the other hand, in the transfer action of the

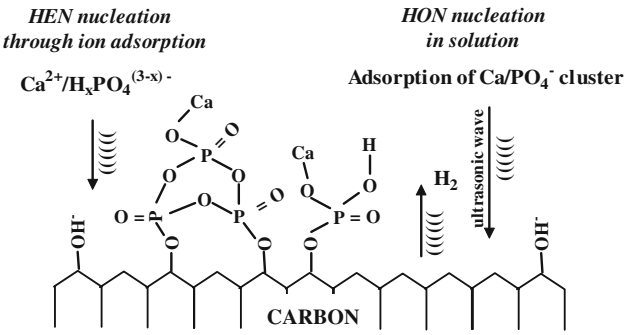

Fig. 5 Scheme of nucleation and growth of calcium phosphate on a cathode carbon surface in the sonoelectrodeposition process

ultrasound and electric field, some CaP precipitates in the solution due to HON will move towards and adhere to the surfaces of the substrate, producing a loose coating. Moreover, the existence of the precipitates will occupy the active positions on the substrate, block the path of the normal deposition and consequently result in reduced deposition efficiency. The resulting coatings are therefore a mixture of adhered precipitates and grown crystal deposits, accounting for the various needle, flake and particle-like microstructures seen.

The chemical composition of the deposits changes with variation in the ionic concentration of the solution. According to FTIR analysis of band intensities, the content of CO_3^{2-} and HPO_4^{2-} groups in the coating increases with corresponding increases in ionic concentration of the solution, while that of PO_4^{3-} decreased [23]. It follows that the lower concentration is favourable for the generation of phosphate (PO_4^{3-}).

It is interesting to note that at every characteristic FTIR peak position, the band intensities are always weaker at 6 mM than at 10 mM, inferring that concentrations less than 10 mM result in less efficient deposition. Additionally, calcium carbonate ($CaCO_3$) crystals are present together with the calcium phosphate coatings. This may be due to the fact that no attempt was made during the sonoelectrodeposition process to prevent CO_2 entering the cell from the atmosphere. However, the presence of $CaCO_3$ is not a disadvantage for the medical application of calcium phosphate coating because it can be converted into calcium phosphate when it is in contact with phosphate ions [5].

5 Conclusions

The deposition of calcium phosphate onto the surface of carbon fabrics has been demonstrated using a sonoelectrochemical method. Chemical and morphological analysis (scanning electron microscopy, FTIR and Raman spectroscopy) revealed that the concentration of calcium and phosphate in the electrolyte solution affected the nature of the crystalline deposits on the material substrate. A mixture of plate, sphere and needle-like deposits was obtained at Ca^{2+} ion concentration greater than 16 mM, however needle-like HA was obtained at lower Ca^{2+} concentrations. The sonoelectrochemical deposition of calcium phosphate appears to consist of two processes, nucleation and crystal growth with heterogeneous nucleation occurring on the surface of the carbon fibres at lower concentrations, leading to the formation of islands of crystal growth over time. It is likely that homogeneous nucleation of calcium phosphate in solution, followed by their adsorption onto the carbon surface accounts for the different coatings observed at higher ionic concentrations. The technique offers advantages over existing HA-coating techniques, which often require higher temperatures or 'line-of-sight' for effective deposition. Sonoelectrochemical deposition may therefore provide a useful way of generating HA coatings on complex carbon-based structures for a wide range of medical device applications.

Acknowledgements The authors gratefully acknowledge the financial support for this project provided through an EU Marie Curie International Incoming Fellowship (EC Contract MIF1-CT-2004-002913) and Mr. A. Blackburn, MAST Carbon Advanced Products Ltd, for providing carbon materials. Thanks are also due to the Scientific Start-up Grant funded by ZhongKai University of Agriculture and Technology (G2360263).

References

1. S.P. Huang, B.Y. Huang, K.C. Zhou, Z.Y. Li, Mat. Lett. **58**, 3582 (2004)
2. A. Stoch, A. Brozek, S. Błazewicz, W. Jastrzebski, J. Stoch, A. Adamczyk, I. Roj, J. Mol. Struct. **651–653**, 389 (2003)
3. M.C. Kuo, S.K. Yen, Mat. Sci. Eng. C **20**, 153 (2002)
4. A. Slosarczyk, M. Klisch, M. Bazewicz, J. Piekarczyk, L. Stobierski, A. Rapacz-Kmita, J. Eur. Ceram. Soc. **20**, 1397 (2000)
5. N. Dumelie, H. Benhayoune, C. Rousse-Bertrand, S. Bouthors, A. Perchet, L. Wortham, J. Douglade, D. Laurent-Maqium, G. Balossier, Thin Solid Films **492**, 131 (2005)
6. Q. Zhanga, Y. Leng, R. Xin, Biomaterials **26**, 2857 (2005)
7. Y. Yang, K. Kim, J. Ong, Biomaterials **26**, 327 (2005)
8. V. Nelea, C. Morosanu, M. Iliescu, I.N. Mihailescu, Appl. Surf. Sci. **228**, 346 (2004)
9. K. Ozeki, T. Yuhta, Y. Fukui, H. Aoki, Surf. Coat.Technol. **160**, 54 (2002)
10. S. BAN, S. Maruno, Biomaterials **19**, 1245 (1998)
11. S. Ban, J. Hasegawa, Biomaterials **23**, 2965 (2003)
12. C.A. Paddon, C.E. Banks, I.G. Davies, R.G. Compton, Ultrason. Sonochem. **13**, 126 (2006)
13. F. Touyeras, J.Y. Hihn, X. Bourgoin, B. Jacques, L. Hallez, V. Branger, Ultrason. Sonochem. **12**, 13 (2005)
14. M.E. Hyde, R.G. Compton, J. Electroanal. Chem. **531**, 19 (2002)
15. H.M. Han, S.V. Mikhalovsky, G.J. Phillips, A.W. Lloyd, New Carbon Mat. **22**, 121 (2007)
16. E. Smith, G. Dent, in *Modern Raman Spectroscopy—A Practical Approach* (John Wiley & Sons Ltd, Chichester, 2005) p. 139
17. D. Kashchiev, G.M. Van Rosmalen, Cryst. Res. Technol. **38**, 555 (2003)

18. J.L. Hardcastle, J.C. Ball, Q. Hong, F. Marken, R.G. Compton, S.D. Bull, S.G. Davies, Ultrason. Sonochem. 7, 7 (2000)
19. H.M. Han, G.J. Phillips, S.V. Mikhalovsky, S. Fitzgerald, A.W. Lloyd, J. Mat. Sci.: Mat. Med. (2007) doi: 10.1007/s10856-007-3337-6
20. X. Lu, Y. Leng, Biomaterials **26**, 1097 (2005)
21. R. Vander Meer, H.T. De Vrvies, Biochem. J. **229**, 265 (1985)
22. S. Rößler, A. Sewing, M. Stölzel, R. Born, D. Scharnweber, M. Dard, H. Worch, J. Biomed. Mat. Res. **64A**, 655 (2002)
23. P. Taddei, A. Tinti, G. Bottura, A. Bertoluzza, Biopolym. (Biospectrosc.) **57**, 140 (2000)